Simultaneous observations of equatorial plasma depletion by IMAGE and ROCSAT-1 satellites

Chin S. Lin,[1] Thomas J. Immel,[2] Huey-Ching Yeh,[3] Stephen B. Mende,[2] and J. L. Burch[4]

Received 5 September 2004; revised 3 March 2005; accepted 23 March 2005; published 11 June 2005.

[1] Simultaneous observations of the equatorial ionosphere by the ROCSAT-1 and IMAGE satellites were used to study zonal propagation characteristics of equatorial plasma bubbles. IMAGE far ultraviolet (FUV) nighttime images have indicated signatures of depression in the brightness of equatorial airglow arcs. Using the list of airglow brightness depression events observed by IMAGE, we surveyed ROCSAT-1 Ionospheric Plasma and Electrodynamics Instrument data and found three ROCSAT-1 passes with simultaneous plasma observations in the same local time sector. Brightness depressions seen in FUV images are found to correlate with equatorial plasma bubbles detected by ROCSAT-1 at 600 km altitude with a separation distance between bubbles varying from 300 to 1000 km. Successive FUV images are averaged to produce a keogram with UT versus longitude, which is then used to deduce zonal drift velocity for plasma density depletions. The drift speed determined from FUV images is compared with ion drift velocities measured by ROCSAT-1. The analysis indicates that the bubbles drift faster than the ambient plasma. The relative zonal velocity of plasma bubbles with respect to the ambient plasma is large, over 200 m/s when plasma bubbles are first created in the early evening hours. The relative zonal velocity decreases rapidly with magnetic local time (MLT) from over 200 m/s at 20 MLT to ~30 m/s at 22 MLT. ROCSAT-1 has detected quasiperiodic structures for equatorial plasma bubbles, corresponding to the quasiperiodic appearance of FUV brightness depression. The quasiperiodic structure of plasma bubbles has been interpreted as evidence of zonal propagation of atmospheric gravity waves with a wavelength in the range of about 300–1000 km. The observed zonal drift velocity of plasma bubbles is shown to be consistent with the horizontal propagation velocity of acoustic gravity waves. The dependence of the horizontal group velocity of acoustic gravity waves on various parameters is further investigated. The vertical wavelength of acoustic gravity waves is found to be the most sensitive parameter for determining the horizontal group velocity of acoustic gravity waves and thus presumably the zonal propagation of equatorial plasma bubbles. The relative zonal propagation of equatorial plasma bubbles might imply strong coupling between atmospheric gravity waves and the Rayleigh-Taylor instability. The obtained results suggest that atmospheric gravity waves play an important role not only for initiating plasma bubbles but also for maintaining the horizontal motion of equatorial plasma bubbles.

Citation: Lin, C. S., T. J. Immel, H.-C. Yeh, S. B. Mende, and J. L. Burch (2005), Simultaneous observations of equatorial plasma depletion by IMAGE and ROCSAT-1 satellites, *J. Geophys. Res.*, *110*, A06304, doi:10.1029/2004JA010774.

1. Introduction

[2] Space-based measurements from the IMAGE far ultraviolet imager (FUV) [*Mende et al.*, 2000] at high apogee allow for global-scale observations of nightside ionospheric densities and structures. The IMAGE/FUV imager, which has a 5-nm passband centered at 135.6 nm for detecting emissions of atomic oxygen, has observed persistent features of the equatorial airglow arcs from the evening terminator to postmidnight local times [*Immel et al.*, 2003]. The airglow arcs are characterized by two longitudinally extended bright bands of atomic oxygen (OI) 135.6-nm emissions, corresponding to a plasma density enhancement on both sides of the magnetic equator. The airglow arcs indicate regions of enhanced plasma densities related to the equatorial anomaly in the low-latitude ionosphere, where most of the emissions are produced within ~100 km altitude of the *F* layer peak.

[1]Institute for Scientific Research, Boston College, Chestnut Hill, Massachusetts, USA.
[2]Space Science Laboratory, University of California, Berkeley, California, USA.
[3]Institute of Space Science, National Central University, Chung-li, Taiwan.
[4]Department of Space Science, Southwest Research Institute, San Antonio, Texas, USA.

0148-0227/05/2004JA010774$09.00

[3] Significantly, IMAGE/FUV nighttime images in the SI-13 channel have indicated signatures of depression in the brightness of equatorial airglow arcs [*Sagawa et al.*, 2003; *Immel et al.*, 2003]. The decrease in airglow brightness is generally believed to be caused by depletions in plasma density in association with plasma bubbles or equatorial spread *F* irregularities [*Kelley*, 1989]. Using keograms of airglow arcs in the coordinate of universal time and magnetic longitude, *Immel et al.* [2003] showed that plasma density depletions were drifting eastward, generally for several hours. They determined the velocity of drifting plasma density depletions to be greatest in the early evening, with peak values about 150–200 m/s in the 20 magnetic local time (MLT) sector, and to decrease by a factor of 2 or more by midnight.

[4] Using the list of airglow brightness depression events studied by *Immel et al.* [2003], we surveyed ROCSAT-1 Ionospheric Plasma and Electrodynamics Instrument (IPEI) data and found three passes in which ROCSAT-1 detected simultaneously equatorial plasma bubbles in the same local time as the IMAGE/FUV images of airglow arcs. In this paper we report simultaneous satellite observations and analysis results from comparing the zonal velocity of the background plasma measured by ROCSAT-1 just outside plasma bubbles with the zonal drift speed of plasma bubbles deduced from the IMAGE/FUV global images. Such a comparison has not been reported before.

[5] Zonal drifts of ionospheric irregularities have been studied using various ground-based measurements including incoherent scatter radar, radio scintillations, airglow images, and GPS measurements [*Abdu et al.*, 1985, 1998; *Basu et al.*, 1996; *de Paula et al.*, 2002; *Fejer et al.*, 1981; *Kil et al.*, 2000; *Sobral and Abdu*, 1990; *Sobral et al.*, 1999; *Valladares et al.*, 1996]. These measurements generally indicate that the apparent eastward zonal velocity of ionospheric plasma depletion is peaked at 2000–2100 LT with the average peak value varying between 150 and 200 m/s. It is generally assumed that irregularities drift in the eastward direction with the same speed as the background plasma. However, because the zonal plasma drift exhibits considerable variability, *Fejer et al.* [1991] argued that the zonal velocities of the equatorial *F* region plasma bubbles in the premidnight sector do not always correspond to the velocity of the ambient plasma.

[6] The ambient plasma drifts in the low-latitude ionosphere have previously been measured by using ion drift meters and vector electric field antennas on board several low-altitude Earth-orbiting satellites including AE-E, DE 2, and San Marco D [*Hanson and Bamgboye*, 1984; *Aggson et al.*, 1987; *Maynard et al.*, 1988; *Coley and Heelis*, 1989; *Fejer et al.*, 1991; *Maynard et al.*, 1995]. The zonal velocity is eastward at night with nighttime values exceeding 100 m/s and an early evening peak of ~170 m/s near 2100 LT. The basic behaviors are similar to those derived from Jicamarca incoherent scatter radar data [*Fejer et al.*, 1991].

[7] In section 2 we describe the IMAGE FUV and ROCSAT-1 plasma data used in this study. Section 3 presents the observations of equatorial plasma bubbles and the data analysis. We discuss the results in section 4 and compare the observed bubble zonal drift speed with the propagation velocity of atmospheric gravity waves in section 5. The conclusion is given in section 6.

2. Data Description

[8] The far ultraviolet imager on board the IMAGE satellite has been used to study the nighttime equatorial airglow arcs on a global scale [*Burch*, 2000; *Mende et al.*, 2000]. The FUV instrument package has three cameras used to image the upper atmosphere at three wavelengths. In this study we examine data from the SI-13 channel, which has a passband centered at 135.6 nm with a 5-nm bandwidth [*Mende et al.*, 2000]. The FUV/SI-13 channel is specifically designed for observing the 135.6-nm emission, which on the nightside comes mostly from recombination of atomic oxygen ions. In the low-latitude nighttime ionosphere the 135.6-nm intensity is mainly determined by the square of the electron density because oxygen ions are the dominant ion species near the *F* layer peak.

[9] The IMAGE satellite was launched in March 2000 into a highly elliptical orbit with perigee and apogee altitudes of 1000 km and 7.2 R_E, respectively. During spring 2002 the local time of IMAGE apogee was in the evening sector, and the FUV imager was able to obtain a clear view of the northern airglow arc from the evening terminator to postmidnight local times. The FUV imaging cadence matches the rotation rate of the satellite (one rotation per 2 min) with an integration time of 5 s per SI-13 image.

[10] The ROCSAT-1 satellite launched in 1999 had a circular orbit with an altitude near 600 km and an orbital inclination angle of 35°. On board the ROCSAT-1 satellite the IPEI payload contained an ion trap, two drift meters, and a retarding potential analyzer [*Yeh et al.*, 1999]. The ion trap sensor measured the total ion density, and the two ion drift meters measured the two perpendicularly cross-track components of ion drift velocities. The retarding potential analyzer (RPA) data are used to infer ion velocity in the satellite ram direction. The three perpendicular components of ion velocity in the satellite frame are then transformed to obtain two perpendicular components of ion convective velocity and the field-aligned flow velocity in the geomagnetic field oriented coordinate system according to the International Geomagnetic Reference Field (IGRF) magnetic field model. The field-aligned velocity, $V_{\|}$, is taken to be positive along the magnetic field direction. The two perpendicular components of ion convection velocity are denoted as V_M and V_Z in this paper. The velocity V_M component is chosen to be perpendicular to the magnetic field on the meridonal plane and positive when it is in the outward direction. Since the V_M velocity component is close to the vertical direction near the equator, it is referred to as the vertical component here. The other velocity component V_Z perpendicular to both V_M and the magnetic field direction is the zonal velocity component, positive in the eastward direction. Because ion drift velocity measurements in the ram direction inside density bubbles could have uncertainties due to fitting of the RPA data, we remove spikes and

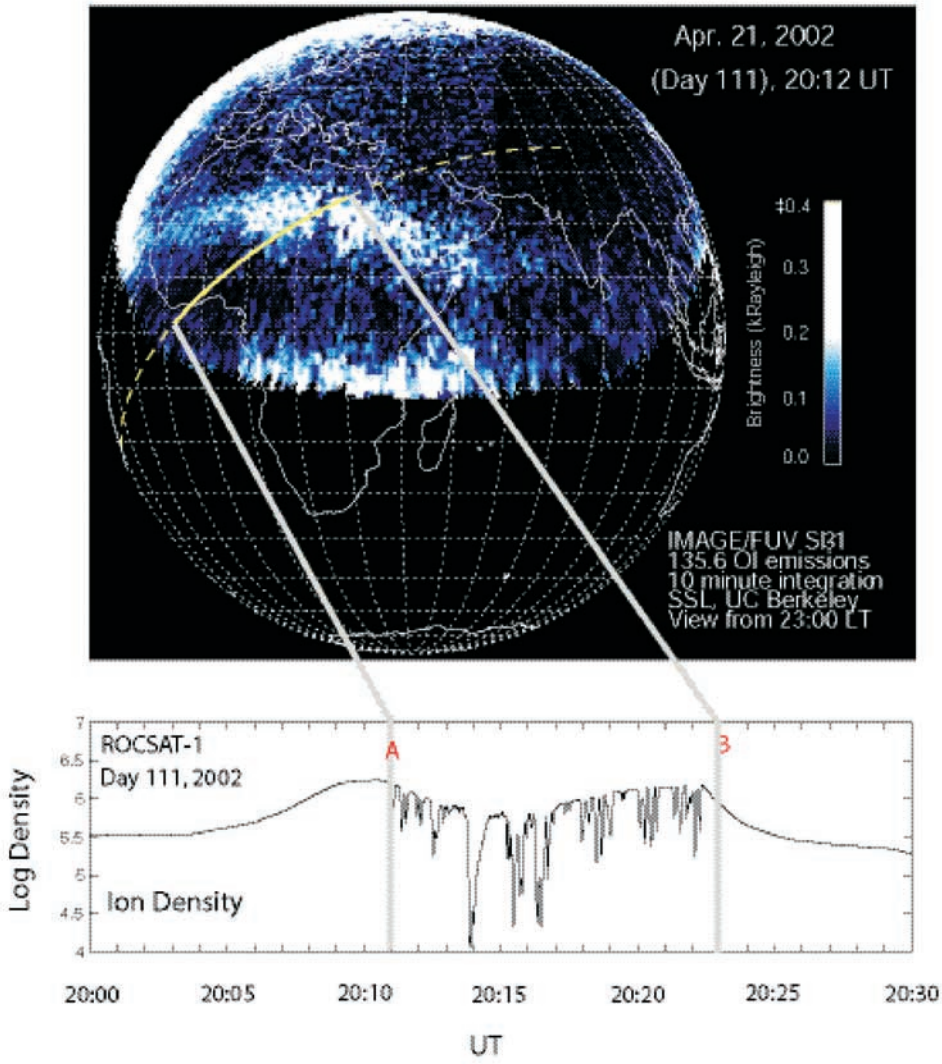

Figure 1. (top) An example of far ultraviolet (FUV) 135.6-nm imaging of airglow arcs mapped onto a projection of geographic coordinates. The time period of the image starts from 2012 to 2022 UT on 21 April 2002. The trajectory of ROCSAT-1 is mapped on the FUV image. The solid line covers the time interval when ROCSAT-1 detected equatorial plasma bubbles, whereas the dashed line represents the satellite trajectory without detecting bubbles. (bottom) Ion density measurements by ROCSAT-1 at 600 km.

apply a moving average to the ram velocity data in this analysis.

3. Observation and Analysis

[11] Figure 1 is a 135.6-nm image of the nightside Earth observed by IMAGE FUV/SI on 21 April 2002 starting from 2012 to 2022 UT. The image is made from integrations of 45-s SI-13 exposures obtained during 8 min of nominal imager operations with 2-min image cadence (Figure 1, top). The two bright horizontal bands display the northern and southern airglow arcs, respectively, as the depletion over Egypt is most obvious around this time. The FUV image shows gaps or brightness decreases in the bands of airglow arc, more distinctly in the southern airglow arc. We have overlaid ROCSAT-1's trajectory on the FUV image with the solid line specifying the period during which ROCSAT-1 observed equatorial plasma bubbles. Figure 1 (bottom) indicates that ROCSAT-1 measured many density depletions from 2012 to 2023 UT. For example, the ion density around 2015 UT dropped from a background of 5×10^5 cm^{-3} to as low as 5×10^4 cm^{-3}. We have identified at least seven distinct plasma bubbles, and their occurrence appears to be periodic.

[12] Moving northward to higher latitudes, ROCSAT-1 detected ion density dropouts between 0° and 25° geographic latitude (Figure 1). ROCSAT-1 did not observe density depletion at southern latitudes in this pass because it was taking measurements at early evening local time (<1930 LT).

[13] To determine the temporal and longitudinal variations in the arc's brightness, we synthesize series of FUV images into a FUV brightness keogram. The FUV images

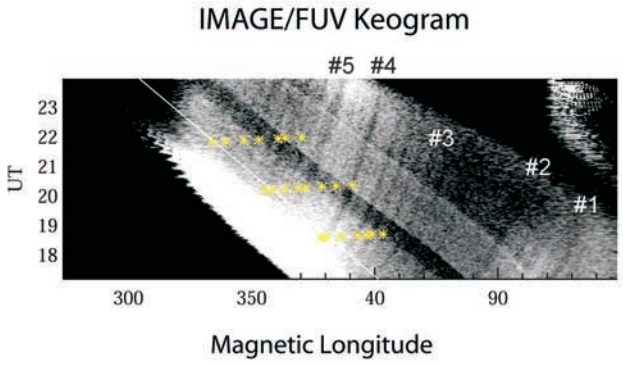

Figure 2. Keogram of the integrated FUV brightness over the northern airglow band that was observed by IMAGE on day 111, 2002. The horizontal scale of the keogram is magnetic longitude, where 0° longitude coincides with Greenwich, and the vertical scale is UT. Yellow asterisks mark the position in the keogram where ROCSAT-1 detects a plasma bubble. Five major tracks with the track numbers shown on them are used to deduce the zonal drift speed of density depletion.

are first mapped to a regularly spaced grid of magnetic longitude and latitude, and then the instrument counts between 0° and 30° magnetic latitude are summed for each bin of longitude in a bin width of 0.5° [*Immel et al.*, 2003; *Sagawa et al.*, 2003]. Here magnetic longitude is defined as the longitude in magnetic coordinates using IGRF model with Greenwich at 0°. The keogram with UT on the vertical axis and magnetic longitude on the horizontal axis for day 111, 2002, is presented in Figure 2. The decreases in the total 135.6-nm emission intensity are revealed as dark tracks, which extend eastward in longitude with increasing UT. From the slope of dark tracks the zonal drift speed of the brightness depression is determined [*Immel et al.*, 2003]. The zonal drift speed deduced for several major tracks is shown in Figure 3, which indicates the zonal drift speed decreasing with MLT. For example, tracks 3, 4, and 5 have the zonal drift speed initially as high as 350 m/s at ~20 MLT and decreasing to ~150 m/s near local midnight.

[14] During the period of Figure 2 the ROCSAT-1 satellite passed through the view of IMAGE FUV instrument. We display each occurrence of plasma bubbles detected by ROCSAT-1 as a yellow asterisk on the keogram. Figure 2 indicates a very good agreement between ROCSAT-1 observation of plasma bubbles and IMAGE observation of brightness depression in airglow arcs.

[15] On the basis of ROCSAT-1 observations alone we generally could not tell if ROCSAT-1 had detected the same plasma bubble in its consecutive passes. However, by mapping locations of plasma bubbles detected by ROCSAT-1 in the IMAGE/FUV keogram (Figure 2) we notice that the first bubble detected on the first pass around 1800 UT and the last plasma bubble detected on the second pass around 2000 UT by ROCSAT-1 may very well be the same plasma bubble (Figure 2). Similarly, the first three density bubbles detected during the second pass appear to be detected by the satellite again during the third pass around 2100 UT as the last three bubbles.

[16] For the depletion track 4 in the FUV keogram, ROCSAT-1 sampled the same density dropout at 1835 UT in the first orbit and 2022 UT in the second orbit, separated by 11.6° in magnetic longitude. From the initial and final positions of this bubble we estimate that it moved at a mean speed of 190 m/s during the time interval. As shown in Figure 3, the initial velocity for track 4 depletion was over 300 m/s when ROCSAT-1 first detected it, much larger than the mean velocity of 190 m/s estimated from the ROCSAT-1 observations. However, the drift speed of depletion decreased rapidly with MLT. By the time ROCSAT-1 observed the bubble again at ~22.4 MLT, the drift speed was reduced to well under 150 m/s. We compute the mean drift speed by taking the time average of drift speed from the keogram over the interval, and we obtain a mean drift speed of ~200 m/s, which is in agreement with the crude estimate based on the ROCSAT-1 detection.

[17] The IMAGE FUV keograms indicate periodic structures of depressed brightness in airglow arcs. The ion density measured by ROCSAT-1 indicates quasiperiodic variation as well (Figure 1, bottom). We have conducted a statistical study of separation distance between distinct plasma density depletion structures observed by ROCSAT-1 during 19–30 April 2002. A total of 180 distinct plasma depletions are identified. We determine the elapsed time ΔT between successive ROCSAT-1 detections of density depletions. For each density depletion structure the time of the maximum density dropout is used to identify the depletion, and secondary density dropouts within the density depletion

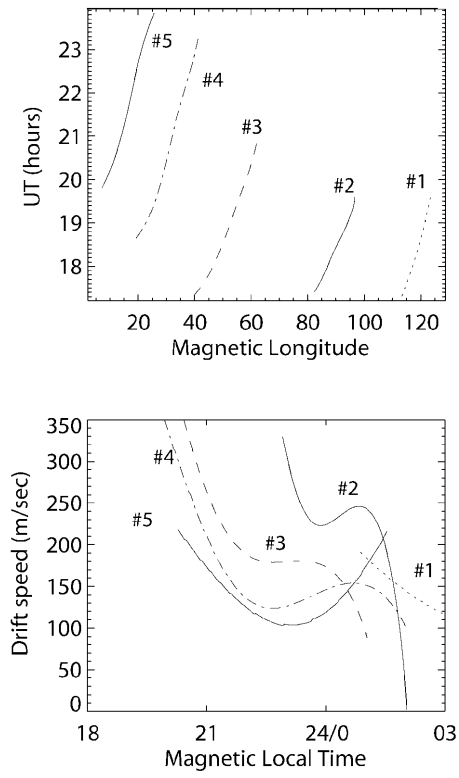

Figure 3. (top) Traces of brightness depression in the keogram and (bottom) the zonal drift speed of plasma bubbles deduced from the traces.

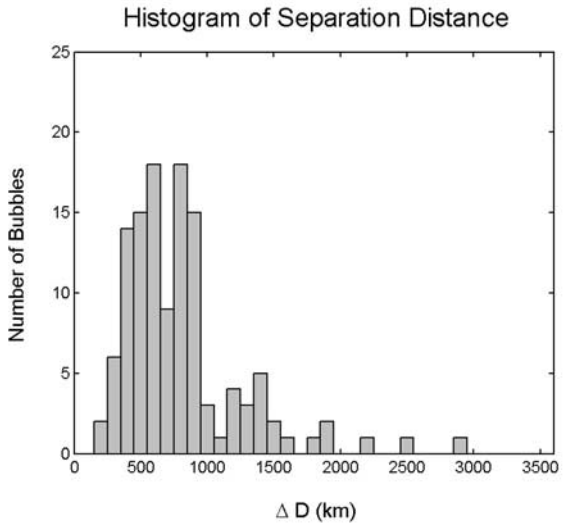

Figure 4. Histogram of the separation distance between plasma density depletions.

are excluded in the statistical study. Since ROCSAT-1's speed (7.5 km/s) is much faster than the drift speed of bubbles, we convert the elapsed time between depletions ΔT into the depletion separation distance ΔD, which is calculated as ΔT times the satellite speed. The subject of density depletion separation distance deserves extensive investigation and a separate paper to describe the study in more details. Here we briefly summarize the pertinent statistical results in the histogram of ΔD, which shows that majority of the separation distance falls between 300 and 1000 km with peaks of the distribution of the separation distance at 600 and 900 km (Figure 4). For the 23 density depletions shown in Figure 2 their separation distance was in the range from 400 to 1100 km.

[18] Figure 5 presents the ion density and three components of ion velocity measured by the ROCSAT-1 IPEI instrument during the interval of the IMAGE/FUV image shown in Figure 1. The IPEI data are plotted as a function of magnetic local time. ROCSAT-1 measured a series of density dropouts between 19.5 and 22.5 MLT (Figure 5, first panel). Figure 5 shows that the vertical component V_M had large spikes associated with the density dropouts before 20.5 MLT, indicating large upward vertical velocities as high as 400 m/s inside the plasma bubbles (Figure 5, second panel). However, V_M was relatively small for plasma bubbles after 20.5 MLT, and it was even negative for the last two bubbles at 22 MLT.

[19] The zonal velocity V_Z is in the range between -200 and $+200$ m/s through the whole pass. Unlike the V_M component it appears that the V_Z magnitude inside the bubbles has no MLT dependence. A careful examination of the V_Z variation reveals that V_Z was positive near both boundaries of the bubbles and negative near the center of bubbles. This means that ions were moving eastward near the boundaries of the bubbles but westward inside the bubbles. Figure 5 (fourth panel) indicates that large flow toward the Southern Hemisphere was observed inside the bubbles.

[20] In Figure 6 we compare the zonal velocity of the background plasma to the zonal drift speed of FUV airglow brightness depression. To focus on the background plasma drift speed, we replot the zonal velocity shown in Figure 5 by omitting the zonal velocity inside the bubbles and connecting the zonal velocity just outside the bubble with the dashed line (Figure 6). The background plasma just outside the bubble increased from -20 m/s at 18 MLT to a

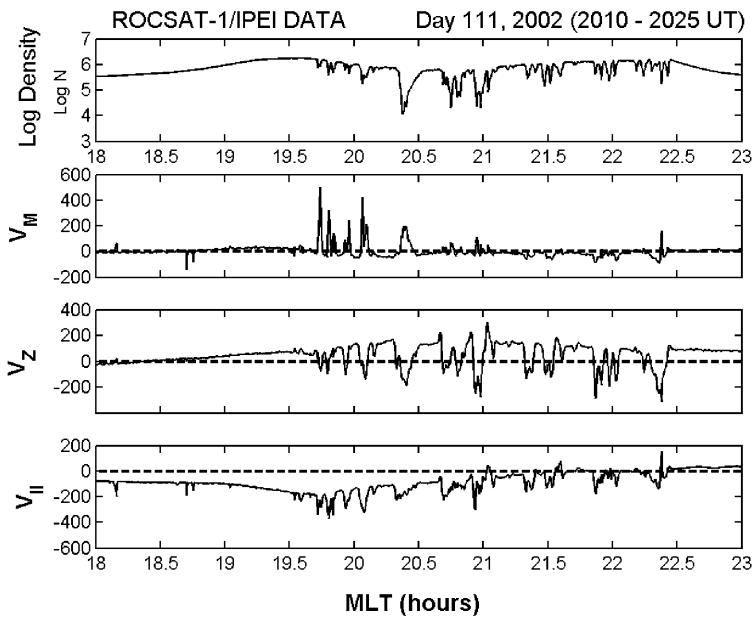

Figure 5. Ion density and three components of ion velocity measured during a ROCSAT-1 pass through plasma bubbles. The V_M component is the vertical component of convective velocity on the meridian plane. The V_Z component is the convective velocity in the zonal direction perpendicular to both V_M and the magnetic field direction. The $V_{||}$ component is the ion field-aligned velocity positive toward north.

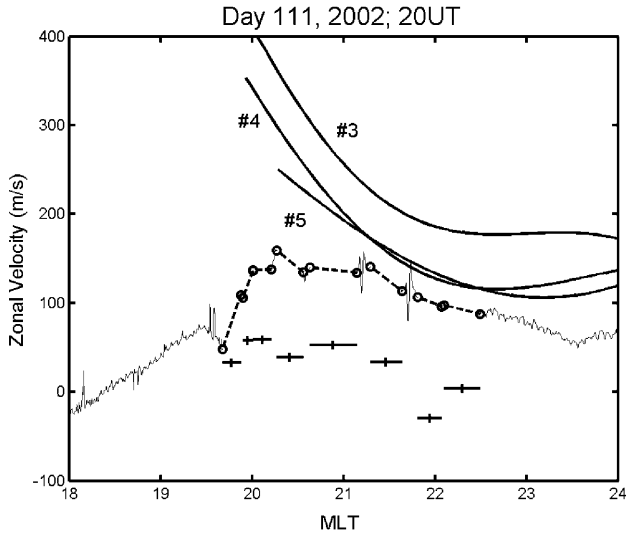

Figure 6. Zonal velocities versus magnetic local time (MLT). The thick solid lines depict the zonal velocity of airglow brightness depression with track number corresponding to those shown in Figure 3. The thin solid line plots the zonal velocity of the background plasma. The zonal velocities of the background plasma just outside the plasma bubbles are presented by open circles. Dashed lines between the open circles connect the zonal velocities at the boundaries of plasma bubbles. The mean zonal velocity inside a bubble is plotted as a horizontal bar with a plus.

high of ~150 m/s at 20 MLT and then decreased gradually to ~50 m/s at 24 MLT. The zonal drift speed of airglow brightness depression for tracks 3, 4, and 5 is plotted for comparison. Figure 6 indicates that the plasma density depletions depicted in the FUV images move much faster than the background plasma.

[21] The ion mean zonal velocity inside the bubbles is presented in Figure 6 as a horizontal bar with a plus at the center. We compute the ion mean zonal velocity inside a bubble as

$$\langle V_Z \rangle = \Sigma n_i V_{Zi} / \Sigma n_i, \quad (1)$$

where the summation over index i is taken over the sampling of density n_i and V_{Zi} inside the bubble. Figure 6 shows that $\langle V_Z \rangle$ varies between zero and 70 m/s, much less than the background plasma zonal velocity just outside the bubbles. This is expected since ions have large negative zonal velocity in the center of the bubbles. It is clear that plasma density depletions associated with airglow arc brightness depression move faster than $\langle V_Z \rangle$.

[22] We summarize the comparison of bubble apparent drift speed with the background plasma zonal velocity for three ROCSAT-1 passes in conjunction with the IMAGE/FUV image (Figure 7). In Figure 7 we present zonal velocity of the background plasma just outside the bubbles as circles connected by dashed lines and the bubble drift speed determined from the IMAGE/FUV keogram as the dotted line. The background plasma zonal velocity has a maximum value of ~150 m/s at ~20 MLT for the first two passes. For the third pass the background plasma zonal velocity is peaked at ~21 MLT with a peak value of 120 m/s. The zonal velocity of the background plasma appears to have no temporal variation from 1800 to 2000 UT. At 2100 UT, ROCSAT-1 detected a decrease in the zonal velocity of the background plasma from the observed values in the previous 2 hours in the MLT range from 19.5 to 21 hours. The zonal velocity of the background plasma seems to be steady after 21 MLT for the three passes.

[23] For all three ROCSAT-1 passes the plasma bubbles appear to travel faster than the background plasma. The velocity difference is large when the bubbles are first detected. For example, the bubble apparent drift speed exceeds 300 m/s around 20 MLT for tracks 3 and 4, whereas the background plasma outside the bubble has a zonal velocity of only ~150 m/s. The difference between the bubble zonal drift speed and the zonal velocity of the background plasma decreases with MLT. At 22 MLT the bubble drift speed is ~140 m/s compared to the background plasma zonal velocity of 100 m/s.

[24] We examine the relative zonal velocity of plasma bubbles as the difference between the zonal drift speed of plasma bubbles and the zonal velocity of the background plasma. The relative zonal velocity could be considered as the zonal velocity of plasma bubbles in the rest frame of the background plasma. For tracks 3 and 4 we deduce the mean zonal velocity of the background plasma using ROCSAT-1 velocity measurements from the passes during 1800 and 2000 UT, since these two ROCSAT-1 passes were in conjunction with tracks 3 and 4. For track 5 we use the zonal velocity measurements from the ROCSAT-1 pass during 2200 UT to represent the background plasma velocity, since this pass was coincident with the track. We first obtain the mean zonal velocity of the background plasma by fitting the zonal velocity of the background plasma as a polynomial function of MLT. The relative zonal velocity is then calculated by taking the difference between the zonal

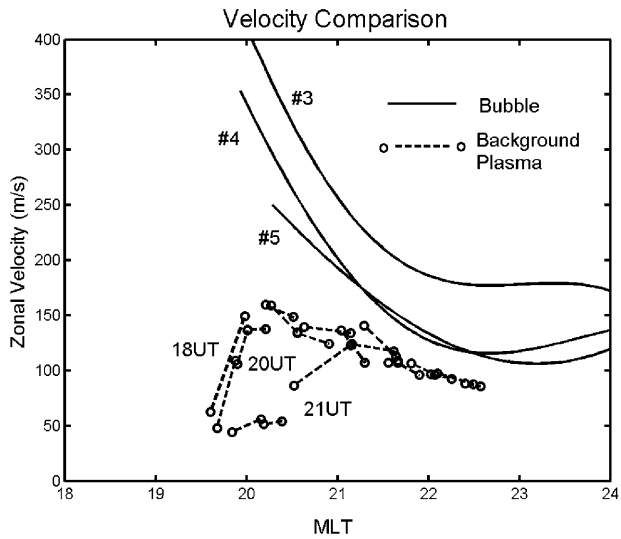

Figure 7. Comparison of bubble drift speed with the background plasma zonal velocity for three ROCSAT-1 passes. The bubble drift speed determined from the IMAGE/FUV keogram is plotted as the solid line. Open circles connected by the dashed lines mark the boundary of plasma bubbles.

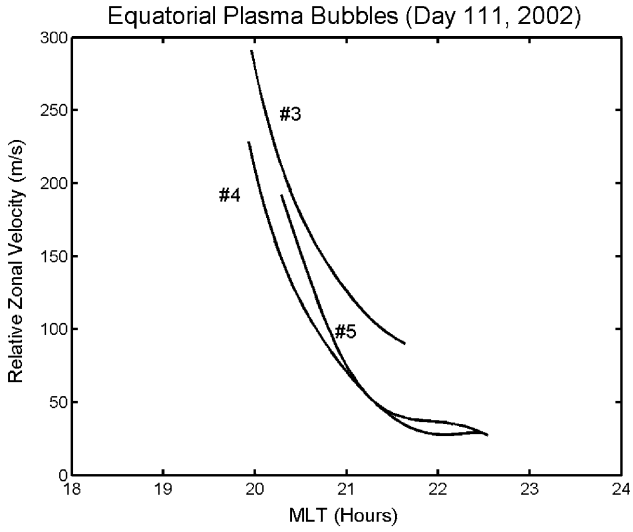

Figure 8. Relative zonal velocity of plasma bubbles with respect to the background plasma as a function of MLT.

drift speed and the mean zonal velocity of the background plasma. Figure 8 indicates that the relative zonal velocity is at maximum when the plasma bubbles are first created in the early evening hours. It decreases rapidly with MLT from over 250 m/s at 20 MLT to ~30 m/s at 22 MLT.

4. Discussion

[25] Space-based measurements from the FUV imager aboard the high-apogee IMAGE satellite allow for global-scale observations of nightside ionospheric densities and structure. At the locations of airglow arc brightness depression seen by the IMAGE FUV imager the ionospheric plasma instrument on board ROCSAT-1 moving at 600 km altitude measured simultaneously low latitude plasma density bubbles. By identifying the localized depressions in the FUV emissions and subsequently tracking their longitude in time we have deduced zonal drift speeds of plasma bubbles. The apparent drift speed of plasma bubbles is compared with the zonal velocity of the background plasma measured just outside the plasma bubbles. The comparison indicates that plasma bubbles appear to move faster than the background plasma in the eastward direction.

[26] Probably because of lack of simultaneous observations of in situ plasma zonal velocity and bubble motion, it is generally believed that plasma bubbles drift with the background plasma zonal velocity [e.g., *Mendillo and Baumgardner*, 1982; *Pimenta et al.*, 2003]. Previously, *Tsunoda et al.* [1982] compared the motion of backscatter plumes measured by the Advanced Research Projects Agency (ARPA) Long-Range Tracking and Identification Radar (ALTAIR) and several radar stations. Their study indicates that plume drift might be faster than the bulk plasma drift by as much as 50%. However, because the backscatter radar measurements were made at significantly different longitudes, they could not reach a definitive conclusion.

[27] The zonal drift velocity determined from the FUV airglow brightness depressions represents the apparent drift velocity of density bubbles between 10° and 15° latitude and 200–300 km altitude since the peak of FUV airglow emission is produced near the F2 peak layer. Although ROCSAT-1 measures ion velocity a few hundred kilometers higher than the F2 peak layer, the relative zonal velocity shown in Figure 8 could not be attributed to the altitude difference in the measurements for two reasons. First, the zonal velocity of the background plasma generally increases with altitude [*Coley and Heelis*, 1989]. According to *Coley and Heelis* [1989, Figure 5] the average zonal velocity in the 18–20 MLT sector is ~50 m/s at 300–400 km altitudes and ~100 m/s at 600 km. So the altitude gradient of the average zonal velocity is in the wrong direction to explain the relative zonal velocity as caused by the altitude difference. Second, the relative zonal velocity before 20 MLT is much larger than the zonal velocity difference between 300 and 600 km. The late evening (22–24 MLT) sector shows a relatively uniform and stable altitude profile of zonal velocity. Therefore the observation that plasma bubbles drift faster than the background plasma could not be accounted for by the altitude difference between the airglow arcs and the velocity measurements by ROCSAT-1.

[28] *Sagawa et al.* [2003] indicates that the zonal drift speed of plasma bubbles has a weak dependence on latitude. Because the zonal velocity determined from IMAGE/FUV keogram has been averaged over latitude, the latitudinal dependence of the relative zonal velocity is thus not examined in this study.

[29] *Immel et al.* [2004] had determined the plasma zonal drift speeds in the nightside ionosphere for nearly 200 plasma bubbles in the March-May period of 2002. The mean drift speed determined by *Immel et al.* [2003] has a peak of 170 m/s at ~20 MLT, which agrees with that deduced from radar observations of equatorial spread *F* [*Fejer et al.*, 1981]. The statistical results of *Immel et al.* [2003] are consistent with *Kil et al.* [2000], who showed that the apparent eastward velocity has a maximum value in 20–21 MLT and then it decreases with MLT.

[30] The apparent zonal drift speed of FUV brightness depression for the events on day 111, 2002, which is in the range 200–300 m/s before 21 MLT, is above the mean value of the survey by *Immel et al.* [2004] in this early evening hours local time (<2100 LT). We have reviewed the local time variation of zonal drift velocity for the plasma bubbles studied by *Immel et al.* [2004]. We found that the bubble events reported here are large but not exceptional when compared to several other cases with high drift speeds found in that survey. In general, high bubble zonal velocity is observed in the first hour after postsunset plasma bubble creation, where thereafter the velocity decreases rapidly with local time. After 2100 LT the zonal velocity indeed decreases to <200 m/s.

[31] The survey by *Immel et al.* [2004] indicates that average zonal drift velocity is higher by 50% in the African–Middle Eastern sector between 60° and 100° longitudes in each MLT sector, where the coordinated bubble observations of day 111 were made. The yet unexplained mechanism for this phenomenon may contribute to the overall high bubble drift speeds described in this report. Also, the bubble events studied here occurred during the recovery phase of the 17–21 April storm when *Kp* values had dropped to relative low values (*Kp* < 2–). *Immel et al.*

[2004] found a clear correlation between drift speeds of bubbles and activity indices such as *Dst* and *Kp* such that zonal drift speeds decrease with increasing *Dst*. These are some factors that may contribute to the fact that the apparent drift speed of plasma bubbles for these poststorm events is higher than the statistical mean.

[32] We have examined the plasma bubble events studied by *Immel et al.* [2004] and conclude that the rapid decrease of zonal drift velocity is common before 2100 LT when plasma bubbles are just formed. It is worthwhile to point out that their presence is faintly exhibited in the FUV images when plasma bubbles show up before 2100 LT. It appears that plasma density depletion might start out weakly during the early times of bubble formation and grow explosively within a short duration. It is arguable whether ground photometer measurements of airglow could have observed the onset. *Sobral et al.* [1999] had analyzed the postsunset zonal drifts of ionospheric plasma depletions in the equatorial and subequatorial regions using 650 days of zonal scanning photometer measurements of the nocturnal OI 630-nm airglow for the period of 1980–1992. The zonal motion of valleys of the OI 630-nm intensity was used to infer the eastward plasma velocity variations with local time. Most of their measurements were taken after 2100 LT. We notice only one survey for the disturbed days during the solar minimum period having photometer measurements before 2000 LT [see *Sobral et al.*, 1999, Figure 1]. For this survey, *Sobral et al.* [1999] reported that the average zonal drift speed decreased rapidly with local time from 200 m/s at 2000 LT to ~100 m/s at 2100 LT. Our results reported here are qualitatively consistent with this ground photometer survey result. Further satellite and ground observations of plasma depletions during the early evening hours are needed to better describe the onset of plasma bubbles.

[33] The relative zonal velocity of plasma bubbles with respect to the background plasma as shown in Figure 8 could be regarded as the group velocity of atmospheric gravity waves in the rest frame of the background plasma. In the framework of our interpretation it seems that atmospheric gravity waves propagate with high velocity initially and slow down with time. The reason for the propagation velocity variation is unclear and remains to be investigated.

[34] *Sagawa et al.* [2003] have earlier reported large-scale (~1000 km) longitudinal wavy structures seen in the IMAGE/FUV images. Such longitudinal wavy structures are evident in the three events studied here, as they appear to be a very common structure seen in the premidnight sector of FUV/SI images regardless of longitude. *Sagawa et al.* [2003] interpreted the periodic structure as caused by zonal propagation of acoustic gravity waves. The ROCSAT-1 observations have indicated quasiperiodic structures of plasma bubbles as well. The separation distance ΔD given in Figure 4 can be interpreted as the horizontal wavelength of atmospheric gravity waves. The range of ΔD suggests the horizontal wavelength of atmospheric gravity waves observed by ROCSAT-1 and IMAGE on day 111, 2002, to be in the range from 300 to 1000 km. This range of horizontal wavelength agrees with the typical wavelength of atmospheric gravity waves, which varies from the atmospheric scale height to the radius of the Earth [*Booker*, 1979].

[35] It has been long recognized that acoustic gravity waves and traveling ionospheric disturbances play a key role in the phenomena of equatorial spread *F* [*Rottger*, 1973; *Booker*, 1979]. *Rottger* [1973] reported large-scale quasiperiodic structures of *F* region irregularities with the median zonal wavelength of 380 km. The close relationship between plasma bubbles and gravity waves has been reported by *Kelley et al.* [1981] and *Hysell et al.* [1990]. Gravity waves can induce electron density fluctuations in the bottomside *F* region through the spatial resonance effect [*Whitehead*, 1971], which occurs when the phase speed of a gravity wave is equal to the plasma drift speed [*Klostermeyer*, 1978]. Several theoretical investigations showed that a zonally propagating gravity wave can initiate the Rayleigh-Taylor instability in the bottomside *F* region [*Huang et al.*, 1993; *Huang and Kelley*, 1996]. After initiation the Rayleigh-Taylor instability amplifies nonlinearly the perturbations induced by the seed gravity wave and produces topside plasma bubbles.

[36] During the evolution from the seeded gravity waves to the nonlinear stage of the Rayleigh-Taylor instability the seeded gravity waves might be destroyed or taken over by the Rayleigh-Taylor instability. In this scenario, plasma bubbles would move with the background plasma since the Rayleigh-Taylor instability has little relative horizontal wave motion with respect to the plasma background. However, if gravity waves have large amplitude before the excitation of the Rayleigh-Taylor instability, it is conceivable that plasma bubbles created by the Rayleigh-Taylor instability might retain the zonal motion of the seeded gravity waves. In this scenario, plasma bubbles would move with the acoustic gravity wave speed relative to the background plasma in agreement with the observations.

[37] To account for the relative zonal propagation of equatorial plasma bubbles, we propose a mechanism that is basically an extension of the Rayleigh-Taylor instability seeded by gravity waves [*Huang and Kelley*, 1996]. We speculate that large amplitude acoustic gravity waves initially propagate zonally in the early evening hours. However, instead of providing small velocity perturbation to seed the Rayleigh-Taylor instability we suggest that these atmospheric gravity waves are strongly coupled to the Rayleigh-Taylor instability, which is then responsible for creating density depletion. Ion drag effects of neutral gas oscillation by acoustic gravity waves could cause a periodic Hall displacement of the charged particles in the *F* region. For acoustic gravity waves propagating perpendicular to the magnetic field the Hall displacement of the charged particles set up periodic polarization electric fields in vertical and zonal directions. Like the seeded gravity wave mechanism for the Rayleigh-Taylor instability, density perturbations of acoustic gravity waves in regions of eastward electric fields are amplified to produce large density depletion when the Rayleigh-Taylor instability condition is satisfied.

5. Acoustic Gravity Waves

[38] The dispersion equation of acoustic gravity waves is known as [*Yeh and Liu*, 1974]

$$k_h^2\left(1-\omega_b^2/\omega'^2\right)+k_z^2=k_o^2\left(1-\omega_a^2/\omega'^2\right). \qquad (2)$$

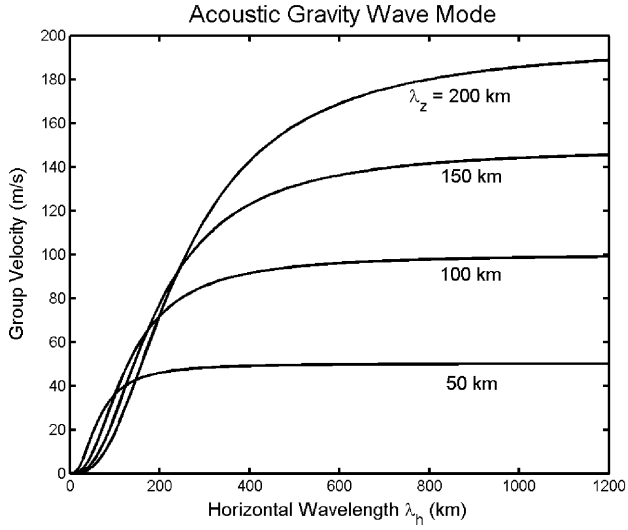

Figure 9. Group velocity of acoustic gravity waves as a function of horizontal wavelength. The horizontal wavelength is in unit of kilometers. The group velocity in unit of m/s is plotted for four values of vertical wavelength. The scale height of neutral gas in the ionosphere is assumed to be 70 km.

In (2), ω' is wave frequency in the frame of neutral wind, k_h is the horizontal wave number, k_z is the vertical wave number, and H is the neutral gas scale height. The parameter $\omega_a = c_s/2H$ is the acoustic cutoff frequency for the scale height H, and ω_b is the buoyancy frequency. In an isothermal atmosphere the buoyancy frequency reduces to $\omega_b = \sqrt{\gamma - 1}\, g/c_s$, where γ is the ratio of specific heats and g is the acceleration of gravity. We also define $k_o = \omega'/c_s$, where c_s is the speed of sound. The wave frequency in the frame of the background plasma is defined as $\omega = \omega' + k_h U_o$, where U_o is the neutral wind horizontal velocity relative to the background plasma. For a gravity wave propagating perpendicular to the magnetic field with frequency $\omega' \ll k_z c_s$ the wave dispersion relation including a horizontal neutral wind becomes [*Klostermeyer*, 1978]

$$\omega = k_h U_o + \frac{\omega_b k_h}{\left(k_h^2 + k_z^2 + 1/4H^2\right)^{1/2}}. \tag{3}$$

The horizontal group velocity $V_g = \partial\omega/\partial k_h$ in the rest frame of the background plasma is then

$$\frac{\partial \omega}{\partial k_h} = U_o + \frac{\omega_b\left(k_z^2 + 1/4H^2\right)}{\left(k_h^2 + k_z^2 + 1/4H^2\right)^{3/2}}. \tag{4}$$

For $k_z \gg 1/2H$ the horizontal group velocity is approximately equal to the horizontal phase velocity. The neutral wind speed U_o relative to the background plasma is believed to be small because the zonal drifts of the ions and the neutrals are generally close because of the F region dynamo and ion drag in the nighttime ionosphere. DE 2 horizontal ion velocity and neutral wind measurements indicate that low-latitude neutral wind speed in the time interval of 18–21 hours is higher than ion horizontal velocity on the average by <20 m/s [*Coley et al.*, 1994].

[39] We calculate the horizontal group velocity of acoustic gravity waves as a function of horizontal wavelength λ_h for $U_o = 0$ (Figure 9). The scale height H is chosen to be 70 km at 300 km altitude according to *Kelley* [1989]. The horizontal group velocity V_g remains almost constant for the horizontal wavelength >400 km. At a given horizontal wavelength the horizontal group velocity increases with the vertical wavelength λ_z. Figure 9 shows that the horizontal group velocity for large λ_h (>400 km) increases from 40 m/s to ~170 m/s when λ_z increases from 50 to 200 km. This range of the horizontal group velocity qualitatively agrees with that observed for the relative zonal drift velocity of plasma bubbles, which varies from 250 m/s at 20 MLT to 20 m/s at 22 MLT (Figure 8). It seems that the agreement might be better when the ions drift faster than the neutral wind ($U_o < 0$).

[40] The group velocity depends on several parameters other than horizontal and vertical wavelengths. We have also examined the dependence of group velocity on the scale height. For the scale height varying in the range of 50–150 km the horizontal group velocity has weak dependence on the scale height. It appears that vertical wavelength is the most sensitive parameter for determining the horizontal group velocity. Figure 10 shows the variation of V_g versus the vertical wavelength λ_z when λ_h = 800 km.

[41] As shown in Figure 8, the relative zonal velocity decreases rapidly with local time in the evening sector. The observed variation of the relative zonal velocity with local time might reflect the dependence of V_g on vertical wavelength λ_z. If this is true, we estimate that vertical wavelength λ_z is ~400 km when acoustic gravity waves are first produced at 19–20 MLT and decreases to <50 km when they propagate to 22 MLT. The estimate of the vertical wavelength is only slightly affected when the relative neutral wind speed is nonzero. The implication of this result to the ionospheric/thermospheric physical processes is that the turbulence of acoustic gravity waves appears to decay

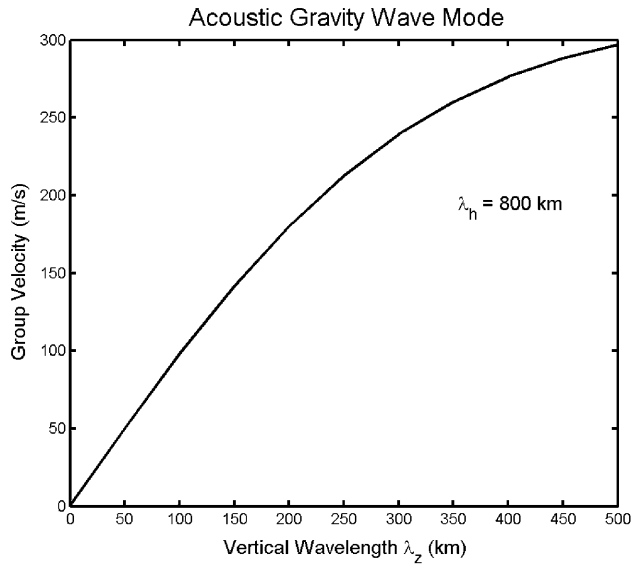

Figure 10. Group velocity of acoustic gravity waves versus vertical wavelength for horizontal wavelength equal to 800 km.

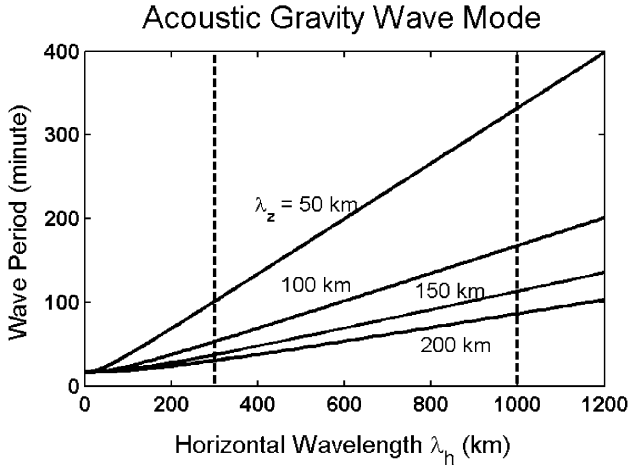

Figure 11. Wave period of acoustic gravity waves as a function of horizontal wavelength for four values of vertical wavelength. The vertical lines at λ_h = 300 and 1000 km represent the limits suggested by the observed separation distance between plasma bubbles.

with time from long wavelength to shorter wavelength. This decay would increase mixing vertically and reduce density perturbations, eventually leading to diminish plasma bubbles in the equatorial ionosphere.

[42] The present analysis may be extended to explain the recurrence rate of plasma bubbles when they are created in the early evening hours. To explore this possibility, we calculate the wave period of acoustic gravity waves for the same horizontal and vertical wavelengths as Figures 9 and 10. Using the group velocity variation shown in Figures 9 and 10, we assume the horizontal wavelength to be ~800 km and the vertical wavelength to be ~200 km when plasma bubbles are first generated. Figure 11 indicates that the wave period of acoustic gravity waves would be ~70 min for the assumed wavelengths. This is consistent with the fact that depletion structures are often observed by ROCSAT-1 on consecutive passes. On the basis of these arguments we speculate that equatorial plasma bubbles are generated with a periodicity of acoustic gravity waves in the early evening hours.

6. Conclusion

[43] Simultaneous observations of the equatorial ionosphere by ROCSAT-1 and IMAGE satellites have been used to study zonal propagation characteristics of equatorial plasma bubbles. The observed drift velocities of plasma bubbles and the background plasma have been examined, and the results indicate that equatorial plasma bubbles drift eastward faster than the background plasma. The observed zonal drift velocity of plasma bubbles is shown to be consistent with the zonal propagation velocity of acoustic gravity waves. Acoustic gravity waves have been known to be the seeded waves for the Rayleigh-Taylor instability, which generates equatorial plasma bubbles. The relative zonal propagation of equatorial plasma bubbles might imply strong coupling between atmospheric gravity waves and the Rayleigh-Taylor instability. The vertical wavelength of acoustic gravity waves appears to be the most sensitive parameter for determining the horizontal group velocity of acoustic gravity waves and thus presumably the zonal propagation of equatorial plasma bubbles. The present work suggests the importance of atmospheric gravity waves in the maintenance of the horizontal motion of equatorial plasma bubbles.

[44] **Acknowledgments.** The present work was supported by NASA SEC-GI grant NNG04GI70G and in part by Air Force contract F19628-02-C-0012 with Boston College. The IMAGE program at Southwest Research Institute was sponsored by NASA contract NAS5-96020, and IMAGE FUV analysis was supported through SwRI subcontract 83820 at the University of California, Berkeley. National Central University received support for this work from National Space Program Office through operation contract NSC92-NSPO (A)-PDD-008-STP01.

[45] Arthur Richmond thanks Eiichi Sagawa and Jose Sobral for their assistance in evaluating this manuscript.

References

Abdu, M. A., I. S. Batista, J. H. A. Sobral, E. R. de Paula, and J. Kantor (1985), Equatorial ionospheric plasma bubble irregularity occurrence on zonal velocities under quiet and disturbed conditions from polarimeter observations, *J. Geophys. Res.*, *90*, 9921–9928.

Abdu, M. A., P. T. Jayachandran, J. MacDougall, J. F. Cecile, and J. H. Sobral (1998), Equatorial *F* region zonal plasma irregularity drifts under magnetospheric disturbances, *Geophys. Res. Lett.*, *25*, 4137–4140.

Aggson, T. L., N. C. Maynard, F. A. Herrero, H. C. Mayr, L. H. Brace, and M. C. Liebrecht (1987), Geomagnetic equatorial anomaly in zonal plasma flow, *J. Geophys. Res.*, *92*, 311–315.

Basu, S., et al. (1996), Scintillations, plasma drifts, and neutral winds in the equatorial ionosphere after sunset, *J. Geophys. Res.*, *101*, 26,795–26,809.

Booker, H. G. (1979), The role of acoustic gravity waves in the generation of spread *F* and ionospheric scintillation, *J. Atmos. Terr. Phys.*, *41*, 501–515.

Burch, J. L. (2000), IMAGE mission overview, *Space Sci. Rev.*, *91*, 1–14.

Coley, W. R., and R. A. Heelis (1989), Low-latitude zonal and vertical ion drifts seen by DE 2, *J. Geophys. Res.*, *94*, 6751–6761.

Coley, W. R., R. A. Heelis, and N. W. Spencer (1994), Comparison of low-latitude ion and neutral zonal drifts using DE 2 data, *J. Geophys. Res.*, *99*, 341–348.

de Paula, E. R., et al. (2002), Ionospheric irregularity zonal velocities over Cachoeira Paulista, *J. Atmos. Sol. Terr. Phys.*, *64*, 1511–1516.

Fejer, B. G., D. T. Farley, C. A. Gonzalez, R. F. Woodman, and C. Calderon (1981), *F* region east-west drifts at Jicamarca, *J. Geophys. Res.*, *86*, 215–218.

Fejer, B. G., E. R. de Paula, S. A. Gonzalez, and R. F. Woodman (1991), Average vertical and zonal *F* region plasma drifts over Jicamarca, *J. Geophys. Res.*, *96*, 13,901–13,906.

Hanson, W. B., and D. K. Bamgboye (1984), The measured motions inside equatorial plasma bubbles, *J. Geophys. Res.*, *89*, 8997–9008.

Huang, C. S., and M. C. Kelley (1996), Nonlinear evolution of equatorial spread *F*: 1. On the role of plasma instabilities and spatial resonance associated with gravity wave seeding, *J. Geophys. Res.*, *101*, 283–292.

Huang, C. S., M. C. Kelley, and D. L. Hysell (1993), Nonlinear Rayleigh-Taylor instability, atmospheric gravity waves, and equatorial spread *F*, *J. Geophys. Res.*, *98*, 15,631–15,642.

Hysell, D. L., M. C. Kelley, W. E. Swartz, and R. F. Woodman (1990), Seeding and layering of equatorial spread *F* by gravity waves, *J. Geophys. Res.*, *95*, 17,253–17,260.

Immel, T. J., S. B. Mende, H. U. Frey, and L. M. Peticolas (2003), Determination of low latitude plasma drift speeds from FUV images, *Geophys. Res. Lett.*, *30*(18), 1945, doi:10.1029/2003GL017573.

Immel, T. J., H. U. Frey, S. B. Mende, and E. Sagawa (2004), Global observations of equatorial ionospheric plasma drift speeds, *Ann. Geophys.*, *22*, 1–9.

Kelley, M. C. (1989), *The Earth's Ionosphere Plasma Physics and Electrodynamics*, Elsevier, New York.

Kelley, M. C., M. F. Larson, C. La Hoz, and J. P. McClure (1981), Gravity wave initiation of equatorial spread *F*: A case study, *J. Geophys. Res.*, *86*, 9087–9100.

Kil, H., P. M. Kintner, E. R. de Paula, and I. J. Kantor (2000), Global Positioning System measurements of the ionospheric zonal apparent velocity at Cachoeira Paulista in Brazil, *J. Geophys. Res.*, *105*, 5317–5327.

Klostermeyer, J. (1978), Nonlinear investigation of the spatial resonance effect in the nighttime equatorial *F* region, *J. Geophys. Res.*, *83*, 3753–3760.

Maynard, N. C., T. L. Aggson, F. A. Herrero, and M. C. Liebrecht (1988), Average low-latitude meridonal electric fields from DE 2 during solar maximum, *J. Geophys. Res.*, *93*, 4021–4037.

Maynard, N. C., T. L. Aggson, F. A. Herrero, M. G. Liebrecht, and J. L. Saba (1995), Average equatorial zonal and vertical ion drifts determined from San Marco D electric field measurements, *J. Geophys. Res.*, *100*, 17,465–17,479.

Mende, S. B., et al. (2000), Far ultraviolet imaging from the IMAGE spacecraft. 3. Spectral imaging of Lyman-α and OI 135.6 nm, *Space Sci. Rev.*, *91*, 287–318.

Mendillo, M., and J. Baumgardner (1982), Airglow characteristics of equatorial plasma depletions, *J. Geophys. Res.*, *87*, 7641–7652.

Pimenta, A. A., J. A. Bittencourt, O. R. Fagundes, Y. Sahai, R. A. Buriti, H. Takahashi, and M. J. Taylor (2003), Ionospheric plasma bubble zonal drifts over the tropical region: A study using OI 630 nm emission all-sky images, *J. Atmos. Sol. Terr. Phys.*, *65*, 1117–1126.

Rottger, J. (1973), Wavelike structures of large scale equatorial spread *F* irregularities, *J. Atmos. Terr. Phys.*, *35*, 1195–1206.

Sagawa, E., T. Maruyama, T. J. Immel, H. U. Frey, and S. B. Mende (2003), Global view of the nighttime low latitude ionosphere by the 135.6 nm OI observation with IMAGE/FUV, *Geophys. Res. Lett.*, *30*(10), 1534, doi:10.1029/2003GL017140.

Sobral, J. H. A., and M. A. Abdu (1990), Latitudinal gradient in the plasma bubble zonal velocities as observed by scanning 630-nm airglow measurements, *J. Geophys. Res.*, *95*, 8253–8257.

Sobral, J. H. A., M. A. Abdu, H. Takahashi, H. Sawant, C. J. Zamlutti, and G. L. Borba (1999), Solar and geomagnetic activity effects on nocturnal zonal velocities of ionospheric plasma depletions, *Adv. Space Res.*, *24*, 1507–1510.

Tsunoda, R. T., R. C. Livingston, J. P. McClure, and W. B. Hanson (1982), Equatorial plasma bubbles: Vertically elongated wedges from the bottomside *F* layer, *J. Geophys. Res.*, *87*, 9171–9180.

Valladares, C. E., R. Sheehan, S. Basu, H. Kuenzler, and J. Espinoza (1996), The multi-instrumented studies of equatorial thermosphere aeronomy scintillation system: Climatology of zonal drifts, *J. Geophys. Res.*, *101*, 26,839–26,850.

Whitehead, J. D. (1971), Ionization disturbances caused by gravity waves in the presence of an electrostatic field and a background wind, *J. Geophys. Res.*, *76*, 238–241.

Yeh, H. C., S. Y. Su, Y. C. Yeh, J. M. Wu, R. A. Heelis, and B. J. Holt (1999), Scientific mission of the IPEI payload on board ROCSAT-1, *Terr. Atmos. Oceanic Sci.*, *9*, suppl., 19–42.

Yeh, K. C., and C. H. Liu (1974), Acoustic gravity waves in the upper atmosphere, *Rev. Geophys.*, *12*, 193–216.

J. L. Burch, Department of Space Science, Southwest Research Institute, 6220 Culebra Road, P.O. Drawer 28510, San Antonio, TX 78228-0510, USA.

T. J. Immel and S. B. Mende, Space Science Laboratory, University of California, Grizzly Peak Boulevard at Centennial Drive, Berkeley, CA 94720, USA.

C. S. Lin, Institute for Scientific Research, Boston College, 140 Commonwealth Avenue, Chestnut Hill, MA, 02467, USA. (chin.lin@bc.edu)

H.-C. Yeh, Institute of Space Science, National Central University, Chung-li 32054, Taiwan.